FLUIDIZED-BED SOLVENT EXTRACTION WITH FORWARD AND COUNTER-CURRENT FLOWS

I. Penchev, A. Minchev, and D. Popova

UDC 536.27:66.061.31.5

A description is given for fluidized-bed extraction with forward and countercurrent flows, variable mass transfer coefficient, and longitudinal mixing. Numerical experiments have been performed for two schemes.

Continuous-running solid-liquid extractors are most commonly of screw type: drum and Hilderband types [1]. New designs have been developed recently [2, 3]. Some of them enable one to operate with countercurrent or forward flows, while others allow only one mode. In design studies, it is necessary to solve a complete model for the extraction on the basis of the relative motion. Up to now, solutions have been obtained only for the solid immobile [4-6], and an incomplete mathematical description has been given for the case of the two media moving, in which the mass transfer coefficients were taken as constant [7]. The model was not solved because there were difficulties due to the two phases being in motion.

Here we give a mathematical description and derive a solution for the extraction that incorporates the speeds of the two phases, the variable mass-transfer coefficient, and the longitudinal mixing.

The diffusion in the bed is described by

$$\varepsilon\left(\frac{\partial C_1}{\partial \tau}+v_z\frac{\partial C_1}{\partial z}\right)+\varepsilon_1(1-\varepsilon)\left(\frac{\partial \overline{C}_2}{\partial \tau}\pm\frac{\partial \overline{C}_2}{\partial z}\right)=\varepsilon D_1\frac{\partial^2 C_1}{\partial z^2}, \tag{1}$$

in which the average concentration of the target component in the solid $\overline{C}_2$ is

$$\overline{C}_2=\frac{T+1}{R^{T+1}}\int_0^R x^T C_2(x,\ \tau)\,dx, \tag{2}$$

in which C_2 is given by

$$\frac{\partial C_2}{\partial \tau}=\frac{1}{x^T}\frac{\partial}{\partial x}\left[x^T D_e(C_2)\frac{\partial C_2}{\partial x}\right]. \tag{3}$$

Equations (1)-(3) are supplemented with the boundary conditions

$$C_{1\text{л}}=C_1(0) \quad \text{at} \quad z=0, \tag{4}$$

$$\frac{\partial C_1}{\partial z}=0 \quad \text{at} \quad z=L, \tag{5}$$

$$\overline{C}_2=C_{20} \quad \text{at} \quad z=L, \tag{6}$$

$$\frac{\partial C_2}{\partial x}=0 \quad \text{at} \quad x=0, \tag{7}$$

$$-\left(\frac{\partial C_2}{\partial x}\right)_{x=R}D_e=k\left(C_2|_{x=R}-C_1\right). \tag{8}$$

Equations (1)-(8) become as follows in dimensionless form:

$$\frac{\partial C_1'}{\partial \tau'}+\frac{v_{00}v_z'}{D_{e0}R}\frac{\partial C_1'}{\partial z'}-\frac{\varepsilon_1(1-\varepsilon)(T+1)}{\varepsilon R^2 D_{e0}}k\left(C_2'|_{x=R}-C_1'\right)-$$

Higher Chemical Engineering Institute, Sofia, Bulgaria. Translated from Inzhenerno-Fizicheskii Zhurnal, Vol. 57, No. 2, pp. 304-308, August, 1989. Original article submitted April 26, 1988.

0022-0841/89/5702-0969$12.50

$$-\frac{\varepsilon_1(1-\varepsilon)v_p' v_{00}}{\varepsilon R}\frac{\partial C_2'}{\partial z'}=\frac{D_1}{D_{e0}}\frac{\partial^2 C_1'}{\partial z'^2}, \tag{9}$$

$$\frac{\partial C_2'}{\partial \tau'}=\frac{1}{x^T}\frac{\partial}{\partial x'}\left(x'^T D_e'\frac{\partial C_2'}{\partial x'}\right), \tag{10}$$

$$C_1'=0 \quad \text{at} \quad z'=0, \tag{11}$$

$$\frac{\partial C_1'}{\partial z'}=0 \quad \text{at} \quad z'=1, \tag{12}$$

$$\frac{\partial C_2'}{\partial x'}=0 \quad \text{at} \quad x'=0, \tag{13}$$

$$\frac{\partial C_2'}{\partial x'}=\mathrm{Bi}\,(\overline{C}_2|_{x=R}-\overline{C}_1'), \tag{14}$$

in which $Bi = kR/D_e$; $D_e' = D_e/D_{e0}$; $C_1' = C_1/C_{20}$; $C_2' = C_2/C_{20}$; $z' = z/R$; $x' = x/R$; $v_z' = v_z/v_{00}$; $v_p' = v_p/v_{00}$; $\tau' = \tau D_{e0}/R^2$.

Equations (9)-(14) were solved by a finite-difference method with an inexplicit five-point scheme [8, 9]. The longitudinal mixing coefficients in certain cases in such screw plant can be quite small, so one gets a small parameter associated with the second derivative in (9), which requires a modified exponential pivot method [10]. The derivative of $\overline{C}_2$ was determined numerically, with the distribution along the bed fitted to a cubic spline [11]. Iteration at each step was used in the refinement for the concentration patterns because of the nonlinearity.

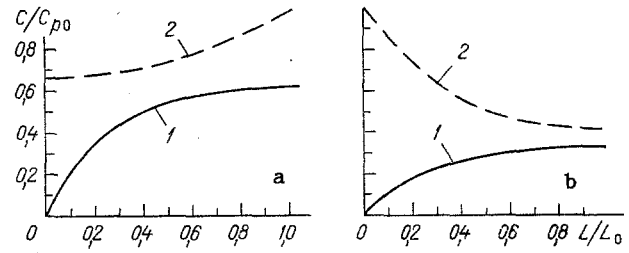

Fig. 1. Target-element concentration variation in the liquid (1) and solid (2) along an apparatus with countercurrent (a) or direct flow (b).

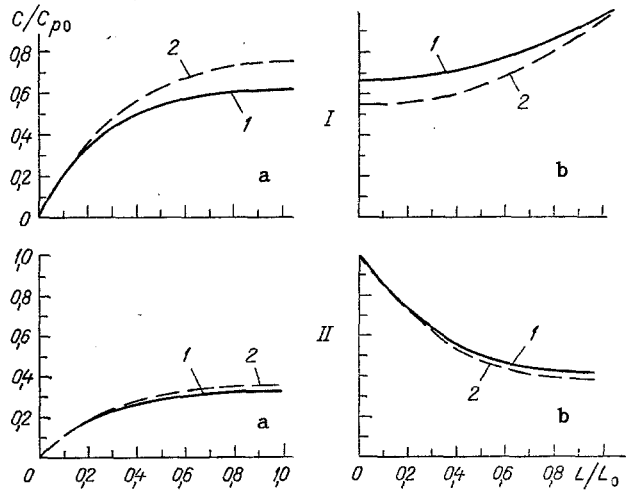

Fig. 2. Concentration variations in the liquid (1) and solid (2) in countercurrent mode (a) and with forward flow (b) for $v_p/v_z = 0.1$ (I) and 0.05 (II); $D_1 = 10^{-19}$ m^2/sec.

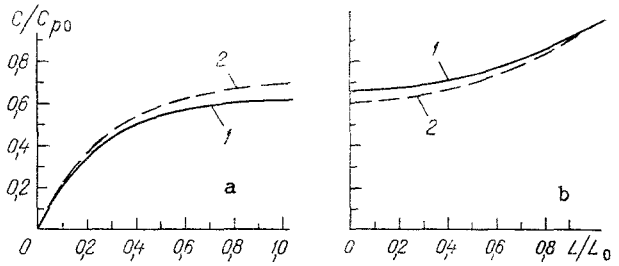

Fig. 3. Concentration variations in the liquid (a) and solid (b) for $D_l = 10^{-19}$ m²/sec (1) and 10^{-12} (2); $v_p/v_z = 0.1$.

Equations close to realistic were used in numerical experiments to determine how the motion of the two media and the longitudinal-mixing coefficients affected the mass transfer; the experiments were done with a variable mass-transfer coefficient in the solid. Figure 1 shows the results, where the definitive parameters corresponded to the experiment described in [12]: grain size set as 10^{-3} m, apparatus length 1 m, mass-transfer coefficient $k = 10^{-5}$ m/sec, and longitudinal mixing coefficient $D_l = 10^{-19}$ m²/sec. The velocity ratio v_p/v_z was taken as 0.1, which corresponded to the [13] data. D_l was taken fairly small, since one can assume for this type of extractor that the longitudinal mixing has little effect. It is true that there are no measurements on this. As would be expected, the concentration in the countercurrent state was much higher than that in the direct-flow one.

Figure 2 illustrates how the velocity ratio affects the concentration profiles in both flow modes; v_p/v_z has much more effect in the countercurrent state.

Figure 3 confirms the suggestion that longitudinal mixing has comparatively little effect on the extraction under countercurrent conditions.

We conclude that the model can be used for a moving-bed extractor over a wide range in the parameters.

NOTATION

ε, bed porosity in m³/m³; ε_1, solid-phase porosity in m³/m³; C_1 and C_2, concentrations of target component in liquid and solid phases in kg/m³; $\overline{C}_2$, mean concentration in solid, kg/m³; τ, time in sec; v_z and v_p, speeds of liquid and solid phases correspondingly in m/sec; z, spatial coordinate along apparatus in m; x, spatial coordinate in solid in m; D_l, longitudinal-mixing coefficient in m²/sec; D_e, mass-transfer coefficient in m²/sec; T, parameter characterizing particle shape; R, particle size in m; $C_{1\ell}$ and C_{20}, initial concentrations in liquid and solid phases correspondingly in kg/m³; k, mass-transfer coefficient in m/sec; C_1' and C_2', dimensionless concentrations in liquid and solid correspondingly; v_{00}, initial speed of liquid in m/sec; τ', dimensionless time; D_{e0}, initial mass conductivity in m²/sec; v_z', v_p', dimensionless speeds of liquid and solid correspondingly; z', dimensionless coordinate along apparatus; x', dimensionless spatial coordinate in solid; Bi, Biot number.

LITERATURE CITED

1. P. G. Romankov and V. I. Kurochkina, Solvent Extraction from Solid Materials [in Russian], Leningrad (1983).
2. E. Shurbert, CLF Patentschrift 604,805 (1977).
3. P. Werner, BRD DE 31 18272A1 (1982).
4. A. Minchev, Iv. Penchev, and I. Kh. Tsibranska, Inzh.-Fiz. Zh., 51, No. 4, 537-541 (1986).
5. A. Minchev, Iv. Penchev, and I. Kh. Tsibranska, Inzh.-Fiz. Zh., 47, No. 4, 636-639 (1984).
6. M. B. Tovbin, B. S. Radkovskii, and Z. M. Tovbina, Ukr. Khim. Zh., 29, No. 11, 1135-1142 (1965).
7. G. A. Aksel'rud and M. A. Al'tshuler, Introduction to Capillary Chemical Technology [in Russian], Moscow (1983).
8. A. A. Samarskii, Difference-Scheme Theory [in Russian], Leningrad (1977).
9. B. Berkovskii and E. F. Nogotov, Difference Methods in Researching Heat Transfer [in Russian], Minsk (1976).

10. E. Dlan, J. Miller, and W. Schilders, Numerical Difference Methods of Solving Boundary-Layer Problems [Russian translation], Moscow (1983).
11. C. de Boer, A Practical Handbook on Splines [Russian translation], Moscow (1985).
12. S. Minkov and A. Minchev, Zh. Prikl. Khim., 59, No. 12, 2704 (1986).
13. P. G. Romankov, N. B. Rashkovskaya, and V. F. Frolov, Mass Transfer in Chemical Engineering [in Russian], Leningrad (1985).

EMISSIVITY MEASUREMENT FOR A CARBON–CARBON COMPOSITE AND A PHENOLIC CARBON PLASTIC

L. S. Slobodkin and M. Ya. Flyaks

UDC 535.231:535.343.2

Two equipments have been used together to determine composite-material emissivity at high temperatures; measurements are reported on the normal emissivities of carbon-based composites.

Carbon–carbon composites and phenolic carbon-filled plastics can be used to make items operating over wide heat-flux ranges, including very high ones [1]. Usually, radiative heat exchange is important, and often decisive, so emissivity data are essential to determine heat transfer and to design components to be subject to intense heat loads. The methods and apparatus for the corresponding measurements are also very important.

The published data on the emissivities of phenolic plastics and carbon–carbon composites are extremely limited and fragmentary [2]. In [3], measurements were reported for $\varepsilon_{\lambda n}$ for a phenol-graphite composite at 2500 K at 0.3-10 μm, while in [4] there are data on the spectral emissivities of coked residues from phenolic carbon at 2550 and 2850 K for 0.4-2.8 μm. There are also data [5, 6] on the emissivities of heat-protective materials based on a carbon–carbon composite with various additives.

Here we describe an apparatus for determining composite emissivities and give measurements on carbon–carbon composites at 700-2000 K.

Two equipments are used in measuring the emissivity at 700-2000 K: one of them is the LIST-5A (Fig. 1a), which is used in determining the temperature dependence of the monochromatic normal-hemispherical reflectivity $\rho_{\lambda n,2\pi}(T)$ in the near IR at 1.0 μm at 700-1400 K and in the visible region at λ = 0.58 μm at 1100-2000 K. The specimen 1 is placed at the center of the integrating sphere 2, which also contains the radiation sources: KI-220-1000 halogen filament lamps and DRT-1000-4 mercury in quartz lamps. The specimen is heated by the beams from the carbon dioxide lasers 6 and 7 working at 10.6 μm. The beam intensities are controlled by the attenuators 9. The recording system consists of the measuring instrument 10 based on an EOP-66 standard optical pyrometer, which is used in the visible region, and the VIMP-015M micropyrometer 5, which makes measurements at 1.0 μm.

One determines $\rho_{\lambda n,2\pi}$ in the visible and near-IR ranges by comparing the radiation fluxex reflected by the specimen and standard; the latter is composed of magnesium oxide deposited on a cassette placed by the specimen at the center. The basic component here is the means of isolating the reflected radiation from the total flux (inherent and reflected). When one determines $\rho_{\lambda n,2\pi}$ at 1.0 μm, the VIMP-015M measures the brightness temperatures of the specimen with the KI-220-1000 lamps on and off and for the standard with the sources on. In order to use the standard pyrometer calibration, the radiation from the object is attenuated if necessary by a filter having transmission τ. The formula is

$$\rho_{\lambda n,2\pi}=\left\{\frac{\tau_{st}}{\tau_s}\exp\frac{C_2}{\lambda}\left(\frac{1}{T'_{st}}-\frac{1}{T'_s}\right)-\frac{\tau_{st}}{\tau_0}\exp\frac{C_2}{\lambda}\left(\frac{1}{T'_{st}}-\frac{1}{T'_i}\right)\right\}\rho^{st}_{\lambda n,2\pi}, \quad (1)$$

Lykov Institute of Heat and Mass Transfer, Belorussian Academy of Sciences, Minsk.
Translated from Inzhenerno-Fizicheskii Zhurnal, Vol. 57, No. 2, pp. 308-313, August, 1989. Original article submitted March 4, 1988.

 0022-0841/89/5702-0972$12.50